Communications of BAO, Vol. 69, Issue 1, 2022, pp. 83-89

Properties of interstellar matter and stellar population in two star-forming regions

E.H. Nikoghosyan *

Byurakan Astrophysical observatory, Byurakan vil., Aragatsotn region, Armenia

Abstract

This study aims to compare the properties of interstellar medium in two star-forming regions with different stellar content, with and without high-mass YSOs. The first region is an extended molecular cloud surrounding five IRAS sources: 05168+3634, 05184+3635, 05177+3636, 05162+3639, and IRAS 05156+3643. The second one is a physically connected pair of ultra compact HII regions, G45.07+0.13 & G45.12+0.13, associated with IRAS 19110+1045 and IRAS 19111+1048 sources, respectively. Using these two star formation regions as an example, one can see the relationship between the initial parameters of the parent molecular cloud (hydrogen column density, dust temperature), the process of star formation itself (external triggering shock or independent condensations), and the parameters of the stellar content. High-mass YSOs were obtained only in the G45.07+0.13 & G45.12+0.13 regions, in which, apparently, the initial density of the parent molecular cloud was higher and the star formation process was initiated by an external triggering shock. In addition, in the IRAS 05168+3634 region, there is a relationship between the density of the interstellar medium and the activity of the star formation process. In those subregions, where the mass and density of the initial, parent molecular cloud is greater, the process of star formation is likely to be more active and have a longer duration. In addition, in these sub-groups, on average, the mass of stars is larger.

Keywords: *infrared: stars – stars: pre-main-sequence, fundamental parameter – ISM: dust, HII regions – ISM: individual objects: IRAS 05168+3634, G45.07+0.13& G45.12+0.13*

1. Introduction

The development of observational astronomy, in particular in the infrared, has largely intensified the study of star-forming regions embedded in gas-dust interstellar matter (ISM), and, consequently, young stellar objects (YSOs) at an early stage of evolution. Nevertheless, despite significant progress, there are significantly much more "white spots" in the theory of star formation than there are answers to questions. However, it is safe to say that stars are formed in dense and cold giant molecular clouds located in the galactic disks (Ambartsumian, 1947, Lada & Lada, 2003). Star formation regions, as a rule, have a complex, multicomponent structure, including genetically interconnected ISM and YSOs (e.g. González-Samaniego & Vazquez-Semadeni, 2020, Pagel & Edmunds, 1981). This necessitates an integrated approach to study of star-forming regions. The integrated approach implies a detailed study and determination of the main properties of already formed young stellar clusters (density, mass function, distribution of evolutionary age, etc.) and the environment (chemical composition, maser emission, density, temperature, etc.).

Often, young stellar clusters or associations have a hierarchical structure both in space and time, i.e. groups of young stars at different stages of evolution may be simultaneously located in one star formation region. In general, the star formation process is a multi-stage, which, moreover, depends on a large extent of the initial conditions in the parent molecular cloud. Previous studies have shown that embedded stellar clusters can tell us a lot about initial star formation scenarios. For example, if the star formation is triggered by external shock, the age spread of new generation stars should be small, while in self-initiated condensations the age spread of young stellar clusters is large (e.g. Preibisch, 2012, Zinnecker & Yorke, 2007). Indeed, many careful studies of star-forming regions find no clear evidence or at most very moderate age spreads of just a few Myr, which is smaller than the crossing time. Such results are in good agreement with and support the scenario of triggered, fast star formation (e.g. Elmegreen et al., 2000).

*elena@bao.sci.am

doi: https://doi.org/10.52526/25792776-22.69.1-83

A special, key place in the theory of star formation is given to high-mass stellar objects. They provide external pressure in the form of expanding HII regions, stellar winds, supernova explosions, and powerful outflows in the surrounding gas, and these factors can initiate a new wave of star formation. Through runaway OB stars, massive star formation can trigger further massive star formation over large (kpc) distances. They are capable of sustaining sequential and self-propagating star formation (Zinnecker & Yorke, 2007) and many previous studies have shown that very often there are dense young stellar clusters in the vicinity of high-mass YSOs (e.g. Azatyan et al., 2016). But at the same time, there are young stellar clusters in which there are no high-mass YSOs. In Ambartsumian (1958) it was suggested that *"... those O-associations contain, as a rule, stars of the T Tauri type, on the other hand, there are T-associations that do not contain hot giants. But, apparently, the mechanisms of star formation in O- and T-associations should be similar. This means that any theory of stellar origin for a given type of association must allow for variations that would provide an explanation for the origin of stars in associations of another type."*

One of the directions of research aimed at understanding the formation of stars of different masses is the study of the ISM properties in the star-forming regions with different stellar composition, with high-mass stellar objects and without. The aim of this work is to compare the properties of the ISM in two star-forming regions with different stellar content, with and without high-mass YSOs.

2. Description of star-forming regions

For a comparative analysis of properties of both the ISM and young stellar content we have chosen two active star-forming regions. The first region is an extended molecular cloud surrounding five IRAS sources: 05168+3634, 05184+3635, 05177+3636, 05162+3639, and IRAS 05156+3643. The second one is a physically connected pair of ultra compact H II (UCHII) regions, G45.07+0.13 and G45.12+0.13, associated with IRAS 19110+1045 and IRAS 19111+1048 sources, respectively. For both regions, detailed studies of both the ISM and the stars were carried out in Azatyan (2019), Azatyan et al. (2022), Nikoghosyan et al. (2021).

The search, identification, and classification of the young stellar population (using the near-, middle, and far-infrared (NIR, MIR, and FIR) photometric data were based on one of the main properties of young stars, namely the infrared excess due to the presence of circumstellar disks and envelopes (Lada & Lada, 2003). Furthermore, the measure of the IR excess in the NIR and/or MIR ranges can be used to characterise the evolutionary stage of a YSO (Class I and Class II). Therefore, YSO candidates can be identified based on their position in colour–colour (c-c) diagrams. The SED fitting tool (Robitaille et al., 2007) was used to determine the main parameters of the stellar objects.

To determine the hydrogen column density $N(H_2)$ and the dust temperature T_d of the ISM, we applied the Modified blackbody fitting on *Herschel* images obtained in four bands: 160, 250, 350, and 500 μm (Hildebrand, 1983). Following the discussion in previous studies (e.g. Battersby et al., 2011) this wavelength range is well applicable to those cases, where the dust temperature is in the range of 5-50 K, while there are no clear restrictions for the column density.

IRAS 05168+3634 region. There are different manifestations of star formation activity in this region: H_2O, NH_3, 44 GHz CH_3OH, and OH maser emission, CS continuum and SiO (J = 2-1) line emission (Varricatt et al., 2010, and ref. therein). Zhang et al. (2005) have discovered a molecular outflow in this region, and Wolf-Chase et al. (2017) - collimated outflows of NIR molecular Hydrogen emission-line Objects (MHOs). According to Sakai et al. (2012) the trigonometric parallax of IRAS 05168+3634 is 0.532 ± 0.053 mas, which corresponds to a distance of $1.88^{+0.21}_{-0.17}$ kpc. Based on the *Gaia* EDR3 database, in Nikoghosyan et al. (2021) it was shown that all IRAS sub-regions belong to the same molecular cloud, which is located at a distance of ~ 1.9 kpc.

Based on the FIR *Herschel* database it was shown that the ISM has an inhomogeneous structure, forming relativity dense clumps around the IRAS sources, which are interconnected by a filament structure (Nikoghosyan et al., 2021). In general, in the sub-regions T_d varies from 11 to 24 K, and $N(H_2)$ - from 1.0 to 4.0×10^{23} cm^{-2}. The masses of the ISM vary from 1.7×10^4 to 2.1×10^5 $M_\odot$. Based on the c-c diagrams, Azatyan (2019) a rich population of embedded YSOs (240 objects) with different evolutionary stages (Class 0/I and Class II) was identified in the sub-regions. The distribution of the stellar members is presented in Fig. 1. The star formation efficiently in the sub-regions is less than 0.1%.

G45.07+0.13 & G45.12+0.13 region. The star-forming regions associated with IRAS 19110+1045

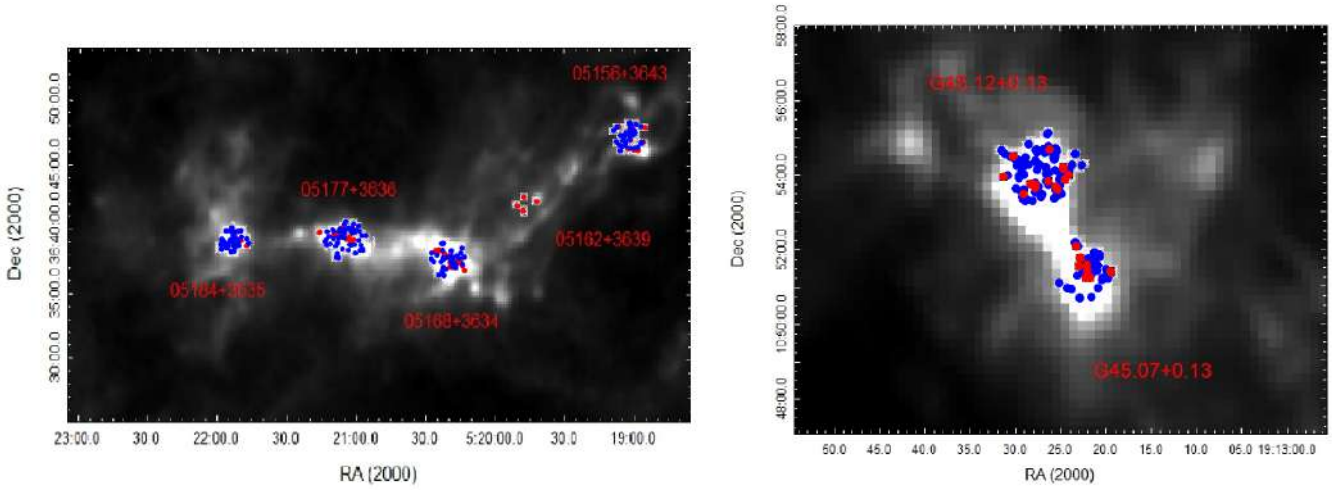

Figure 1. Distribution of YSOs on the *Herschel* 500 μm images (*left panel*: the IRAS 05168+3634 region and *right panel*: the G45.07+0.13 & G45.12+0.13 region). Class I and Class II objects are indicated by filling red and blue circles, respectively.

and IRAS 19111+1048 sources are designated as G45.07+0.13 and G45.12+0.13 UCHIIs, respectively (Wood & Churchwell, 1989). The regions are part of the Galactic Ring Survey Molecular Cloud (GRSMC) 45.46+0.05. The cloud is a large star formation complex (Simon et al., 2001) that hosts several other UCHII regions. Thus, this complex is an ideal laboratory for studying the early stages of massive star formation and their impact on the natal environment. Multi-wavelength studies suggest that both UCHIIs are sites of active massive star formation. In Hunter et al. (1997) CO(J = 6–5) map is presented, which shows bipolar outflows with an origin well centred on the radio position of both UCHIIs. Both regions contain the probe of massive star-forming clumps, SO 30GHz emission, type-I OH masers, but only G45.07+0.13 produces H_2O and methanol maser emissions (Varricatt et al., 2010, and ref. theirin). The distance of the region obtained by the trigonometric parallax method is 7.75 ± 0.45 kpc (Wu et al., 2019).

Using the Modified blackbody fitting on the *Herschel* images it was found that $N(H_2)$ varies from 3.0×10^{23} to 5.5×10^{23} cm^{-2} within the G45.07+0.13 and G45.12+0.13 regions (Azatyan et al., 2022). The maximum T_d values are 35 K in G45.12+0.13 and 42 K in G45.07+0.13. The gas plus dust mass value in G45.12+0.13 is $3.4 \times 10^5 \dot{M}_\odot$ and $1.7 \times 10^5 \dot{M}_\odot$ in G45.07+0.13. The UCHII regions are connected through a cold ($T_d = 19$ K) bridge. The radial surface density distribution of the identified YSOs exhibits dense, embedded in these two physically connected UCHII regions, clusters in the vicinity of both IRAS sources (see Fig. 1 right panel). In total, 37 objects were identified in G45.07+0.13, 87 and in G45.12+0.13.

3. Comparative analysis of two star-forming region

Thus, based on the data obtained in previous works, these two active star-forming regions differ significantly in their stellar content. The properties of stellar objects in the regions are shown in the Fig. 2, which presents colour-magnitude (c-m) diagrams, K luminosity functions (KLFs), as well as the histograms of the distribution of stellar objects by colour index $(J-K)_0$, which, in fact, reflects the evolutionary stage of YSOs. The tables 1 and 2 present generalized data of both the stellar members and the surrounding ISM in the clusters (sub-region's radius, YSOs number, surface stellar density, percent of younger YSOs with Class I evolutionary stage, α slope of KLF, ranges of stellar masses, hydrogen column density. and dust temperature, as well as ISM mass).

IRAS 5168+3634 star-forming region. The c-m diagram of this region suggests an existence of a very young stellar population (see Fig. 2 left panel). But at the same time, we can see that the stellar members have a wide spread relative to the isochrones. Among the objects there are both ZAMS stars and YSOs younger than 0.1 Myr. On the $(J-K)_0$ histogram, the objects are distributed fairly evenly. The α slopes of the KLF of the sub-regions are in the range from 0.12 to 0.21. According to the values of the α slopes, the evolutionary age of the sub-regions can be estimated at 0.1–3 Myr. Therefore, we can conclude that the evolutionary age spread of the stellar objects is large. Moreover, this is true both for the cluster as

doi: https://doi.org/10.52526/25792776-22.69.1-83

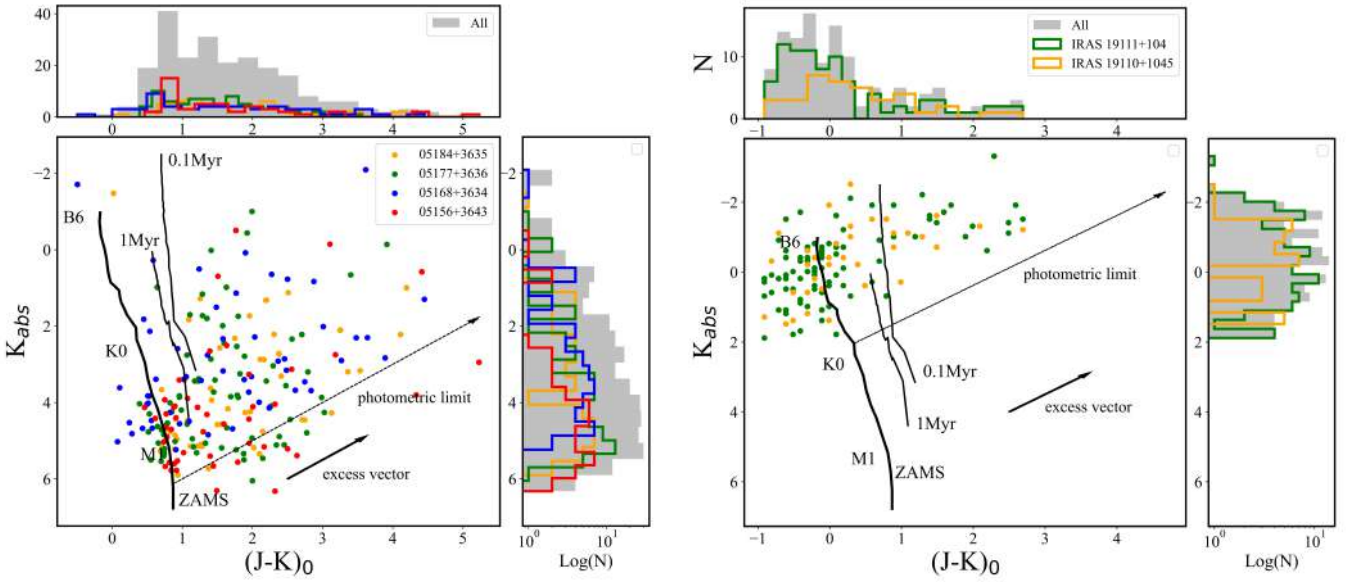

Figure 2. K_{abs} vs. $(J–K)_0$ colour-magnitude diagrams for identified YSOs in the considered regions (*left panel*: the IRAS 05168+3634 region and *right panel*: the G45.07+0.13 & G45.12+0.13 region). The PMS isochrones for the 0.1 and 1 Myr and ZAMS are drawn as solid thin and thick lines, respectively (Siess et al., 2000). The positions of a few spectral types are labelled. The solid arrows indicate the average slope of NIR excesses caused by circumstellar discs (López-Chico & Salas, 2007). The dashed arrows indicate the photometric limit of the UKIRT Infrared Deep Sky Survey in K-band. *Top and right panels* present the histograms of $(J-K)_0$ and K_{abs} values, respectively.

a whole and for sub-groups separately. At the same time, according to the previous studies, no high-mass YSOs were found in this region, but only low- and intermediate-mass. This fact is also reflected by the KLF. Using the SED fitting tool in Azatyan et al. (2022) the spectral energy distributions (SEDs) are constructed for ∼50% of the revealed YSOs. Their parameters are correlated well with the conclusions drawn from the c-m diagram and the KLF.

G45.07+0.13 & G45.12+0.13 region.. In contrast to the previous region, about 75% of stellar objects in the IRAS 19110+1045 and IRAS 19111+1048 clusters are located to the left of the 0.1 Myr isochrone and concentrated around the ZAMS (See Fig. 2 right panel). That also reflects the distribution of the objects on the $(J-K)_0$ histogram. In Azatyan et al. (2022) it was shown that about 75% of the YSOs belonging to the IRAS clusters have an evolutionary age greater than 10^6 yr. Therefore, in general, the evolutionary age spread of the vast majority of stellar objects in the both clusters is small. The distribution of their evolutionary ages is only several Myr years. At the same time, on average the spectral types of stellar members are earlier and, accordingly, their masses are higher (see Table 2). The clusters include several high-mass stellar objects. The α slope of the KLF agrees well with a Salpeter-type initial mass function (IMF) ($\gamma = 1.35$) for a high mass range (O–F stars, $\beta \sim 2$) at 1 Myr.

Table 1. Parameters of the stellar content and ISM in the IRAS 05168+3634 region

Parameter/IRAS	**05156+3643**	**05168+3634**	**05177+3636**	**5184+3635**
Radius (arcmin)	2.8	3.0	3.5	2.5
YSOs' number	47	57	79	52
n_{star} (arcmin^{-2})	1.9	2.0	2.1	2.6
Class I (%)	20	43	28	21
α slope of KLF	0.15	0.21	0.20	0.12
Stellar masses ($M_\odot$)	0.2–1.6	0.5–2.5	0.2–2.2	0.3–1.5
$N(H_2)$ (x10^{23} cm^{-2})	1.1–1.6	1.1–3.8	1.1–2.3	1.1–1.5
T_d (K)	11–12	11–24	12–13	12–15
ISM Mass ($M_\odot$)	1.7×10^4	2.1×10^5	9.2×10^4	4.0×10^4

Table 2. Parameters of the stellar content and ISM in the G45.07+0.13 & G45.12+0.13 region

Parameter/IRAS	**19110+1045**	**19111+1048**
Radius (arcmin)	0.8	1.2
YSOs' number	37	87
n_{star} (arcmin^{-2})	18.4	19.2
Class I (%)	22	16
α slope of KLF	0.21	0.24
Stellar masses ($M_\odot$)	3.2–7.9	3.1–12.6
$N(H_2)$ (x10^{23} cm^{-2})	3.0–5.0	3.0–5.5
T_d (K)	13–42	13–35
ISM Mass ($M_\odot$)	1.7×10^5	3.4×10^5

Properties of the ISM. According to the data presented in the Tables 1 and 2 it is clear that the clusters differ not only in the properties of the stellar content, but also in the properties of the environment, namely, the values of $N(H_2)$ and T_d. In the UCHIIs the values of both parameters are noticeably larger. The higher temperature appears to be directly related to the mass, and hence the temperature, of the stellar members. The presence of high-mass stars causes a higher temperature of the environment in the G45.07+0.13 & G45.12+0.13 region. The higher column density appears to be due to the initial conditions of the parent molecular cloud. It can be assumed that the initial high density was one of the necessary conditions for the formation of high-mass stars.

We would like to draw your attention to one more fact. As we noted above the infrared excess of YSOs, is usually caused by the presence of circumstellar disks. López-Chico & Salas (2007) shown that by incorporating theoretical models of accreting disks, the excess effect on the c-m diagram can be accurately represented by approximately constant slope vectors for disks around Class II T Tauri stars. The coordinates of the vector are (1.01, -1.105) and (1.676, 1.1613) in magnitude units. More massive YSOs are usually much more embedded than T Tauri stars, thus, this correction is unlikely to apply to such objects. However, the presence of a spherical envelope around the disc should cause a greater decrease in J-K for the same variation in the K than in the case of a "naked" disc (Cesaroni et al., 2015). Accordingly, the correction in López-Chico & Salas (2007) can be used to obtain the photometric limit, and therefore lower limit of stellar mass in the region. Using the excess vector we determined the photometric limit of the UKIRT Infrared Deep Sky Survey (UKIDSS) data represented by the dashed arrow in the diagram. It should be noted that for c-m diagram the NIR data from UKIDSS database were used. The arrow is parallel to the excess vector and passes through the ZAMS point with coordinates (0.34, 2.05). The Y-coordinate corresponds to the photometric limit of UKIDSS in the K band (18.02 mag) corrected for distance (7.8 kpc) and interstellar extinction ($A_v = 1.3$ mag, (Azatyan et al., 2022)). In turn, photometric limit K = 2.05 mag corresponds to the ZAMS stars with $\sim 1.4\,M_\odot$ (Siess et al., 2000).

The c-m diagram shows that the cluster members are well above the photometric limit. Indeed, no objects with a mass equal to or less than $1.4\,M_\odot$ were found in Azatyan et al. (2022). For comparison, it should be noted that no such phenomenon is observed in the IRAS 5168+3634 region. There are a significant number of stellar objects here, which are not only concentrated around the vector of the photometric limit (in this region, it is equal to 6.1 mag in K band or $\sim 0.4\,M_\odot$), but also below it.

There are several explanations for this so-called "low-mass deficit". First, the significant distance of the region (8 kpc), which undoubtedly imposes a lower limit on the mass of identified stellar objects. Undoubtedly, the remoteness of the region affected the final result. But at the same time, the question arises why, in contrast to another region, on the c-m diagram there are practically no objects localize directly around the vector of the photometric limit. In addition, according to preliminary results in the neighboring GRSMC 045.49+00.04 region located at the same distance, we were able to identify objects with a much lower mass. Of course, errors in determining the mass also affected the final result. A comparison of model predictions for pre-main sequence stars with robust dynamical mass measurements shows that mass errors at the 30–50% level are typical (Hillenbrand & White, 2004). In Bastian et al. (2010) and Hopkins (2018), a number of other reasons (apart from measurement and modeling errors) due to which there is a shortage of low-mass stellar objects in various clusters. Among them is the unusually high frequency of binary. In addition, the most massive stars in large young clusters are often located in the innermost regions of the

cluster. This phenomenon is known as "mass segregation". Mass segregation is primordial when massive stars form predominantly at the center of the cluster potential. As a result, regions of high density within a star-forming cloud produce a larger proportion of massive stars than regions of lower density. One more reason was be pointed out, namely, the evaporation of low-mass stars. However, this mostly applies to relatively old clusters. In all cases, this issue requires a more detailed study based on a larger sample.

4. Summarizing

As already mentioned above, the stellar populations in young clusters, namely the distribution of their evolutionary age, carry information about how the process of star formation in their parent molecular cloud was initiated. If the star formation was initiated by an external impact, the age spread of new generation stars should be small, while in self-initiated condensations the age spread of young stellar clusters is large. The formation of the two young star clusters we have considered occurred exactly according to different scenarios. The generation of star clusters in the G45.07+0.13& G45.12+0.13 regions were apparently initiated by an external trigger impact, and star formation proceeded very rapidly. On the contrary, independent condensations occurred in the IRAS 5168+3634 region. Moreover, star formation took place sequentially, so the distribution of the evolutionary age of stars is wide. On the other hand, high-mass YSOs were obtained only in the G45.07+0.13& G45.12+0.13 UCHII regions, in which, apparently, the initial density of the parent molecular cloud was higher. Thus, based of the foregoing, we can conclude that the formation of high-mass stars can be initiated in regions with a higher initial density, and at the same time proceed relatively quickly. The latter is more probable when the star formation process is initiated by an external impact. This conclusion is in good agreement with the generally accepted view (Motte et al., 2018).

A certain relationship between the parameters of the stellar population and the properties of the interstellar medium is also seen in the IRAS 5168+3634 region, where the star formation process, probably, have self-initiated, sequential condensation nature. The sub-regions with the highest $N(H_2)$ and interstellar medium mass have the largest percentage of young stellar objects with Class I evolutionary stage. In those sub-regions where the mass and density of the initial, parent molecular cloud is greater, the star formation process is likely to be more active and has a longer duration. In addition, in these groups, on average, the mass of stars is also greater.

Acknowledgements

This work was made possible by a research grant number № 21AG-1C044 from Science Committee of Ministry of Education, Science, Culture and Sports RA.

References

Ambartsumian V. A., 1947, The evolution of stars and astrophysics. Izdatel'stvo Akad Nauk Arm SSR, Erevan

Ambartsumian V. A., 1958, Reviews of Modern Physics, 30, 944

Azatyan N. M., 2019, Astron. Astrophys. , 622, A38

Azatyan N. M., Nikoghosyan E. H., Khachatryan K. G., 2016, Astrophysics, 59, 339

Azatyan N., Nikoghosyan E., Harutyunian H., Baghdasaryan D., Andreasyan D., 2022, Pub. of the Astron. Soc. of Australia, 39, e024

Bastian N., Covey K. R., Meyer M. R., 2010, Ann. Rev. Astron. Astrophys. , 48, 339

Battersby C., et al., 2011, Astron. Astrophys. , 535, A128

Cesaroni R., et al., 2015, Astron. Astrophys. , 581, A124

Elmegreen B. G., Lada C. J., 1977, Astrophys. J. , 214, 725

Elmegreen B. G., Efremov Y., Pudritz R. E., Zinnecker H., 2000, in Mannings V., Boss A. P., Russell S. S., eds, Protostars and Planets IV. p. 179 (arXiv:astro-ph/9903136)

González-Samaniego A., Vazquez-Semadeni E., 2020, Mon. Not. R. Astron. Soc. , 499, 668

Hildebrand R. H., 1983, Q. J. R. Astron. Soc. , 24, 267

Hillenbrand L. A., White R. J., 2004, Astrophys. J. , 604, 741

Hopkins A. M., 2018, Pub. of the Astron. Soc. of Australia, 35, e039

Hunter T. R., Phillips T. G., Menten K. M., 1997, Astrophys. J. , 478, 283

Lada C. J., Lada E. A., 2003, Ann. Rev. Astron. Astrophys. , 41, 57

Lee H.-T., Chen W. P., 2007, Astrophys. J. , 657, 884

López-Chico T., Salas L., 2007, Rev. Mex. Astron. Astrofis. , 43, 155

Motte F., Bontemps S., Louvet F., 2018, Ann. Rev. Astron. Astrophys. , 56, 41

Nikoghosyan E. H., Azatyan N. M., Andreasyan D. H., Baghdasaryan D. S., 2021, Astrophys. Space. Sci. , 366, 114

Pagel B. E. J., Edmunds M. G., 1981, Ann. Rev. Astron. Astrophys. , 19, 77

Preibisch T., 2012, Research in Astronomy and Astrophysics, 12, 1

Robitaille T. P., Whitney B. A., Indebetouw R., Wood K., 2007, Astrophys. J. Suppl. Ser. , 169, 328

Sakai N., Honma M., Nakanishi H., Sakanoue H., Kurayama T., Shibata K. M., Shizugami M., 2012, Publ. Astron. Soc. Jpn. , 64, 108

Siess L., Dufour E., Forestini M., 2000, Astron. Astrophys. , 358, 593

Simon R., Jackson J. M., Clemens D. P., Bania T. M., Heyer M. H., 2001, Astrophys. J. , 551, 747

Varricatt W. P., Davis C. J., Ramsay S., Todd S. P., 2010, Mon. Not. R. Astron. Soc. , 404, 661

Wolf-Chase G., Arvidsson K., Smutko M., 2017, Astrophys. J. , 844, 38

Wood D. O. S., Churchwell E., 1989, Astrophys. J. Suppl. Ser. , 69, 831

Wu Y. W., et al., 2019, Astrophys. J. , 874, 94

Zhang Q., Hunter T. R., Brand J., Sridharan T. K., Cesaroni R., Molinari S., Wang J., Kramer M., 2005, Astrophys. J. , 625, 864

Zinnecker H., Yorke H. W., 2007, Ann. Rev. Astron. Astrophys. , 45, 481

Zinnecker H., McCaughrean M. J., Wilking B. A., 1993, in Levy E. H., Lunine J. I., eds, Protostars and Planets III. p. 429